FREE AND CONSTRAINED MOTION TELEOPERATION VIA NATURALLY-TRANSITIONING RATE-TO-FORCE CONTROL

Robert L. Williams II
Jason M. Henry
Mark A. Murphy
Department of Mechanical Engineering
Ohio University
Athens, OH

Daniel W. Repperger
AFRL / HECP
Wright-Patterson AFB, OH

1999 IEEE International Conference on Robotics & Automation
May, 1999

Contact author information:
Robert L. Williams II
Assistant Professor
Department of Mechanical Engineering
257 Stocker Center
Ohio University
Athens, OH 45701-2979
phone: (740) 593 - 1096
fax: (740) 593 - 0476
email: bobw@bobcat.ent.ohiou.edu
URL: http://www.ent.ohiou.edu/~bobw

FREE AND CONSTRAINED MOTION TELEOPERATION VIA NATURALLY-TRANSITIONING RATE-TO-FORCE CONTROL

Robert L. Williams II, Jason M. Henry, Mark A. Murphy
Mechanical Engineering
Ohio University
Athens, OH 45701

Daniel W. Repperger
AFRL / HECP
Wright-Patterson AFB, OH 45433

ABSTRACT

The Naturally-Transitioning Rate-to-Force Controller (*NTRFC*) is presented for remote teleoperation of manipulators. Our goal is to provide a single controller which handles free motion, constrained motion, and the transition in-between without any artificial changes. In free motion the displacement of the master device (via the human operator's hand) is proportional to the commanded Cartesian rate of the remote manipulator. In contact the displacement of the human operator's hand is proportional to the wrench (force/moment) exerted on the environment by the remote manipulator. The transition between free rate motion and applied-wrench contact with the environment requires no changes in control mode or gains and hence is termed natural. Furthermore, in contact, if the master enables force reflection, the wrench of the human operator's hand exerted on the master is proportional to the wrench exerted on the environment by the remote manipulator. This paper demonstrates the *NTRFC* concept via a simple 1-dof model and then discusses experimental implementation and results from a remote Merlin manipulator teleoperated via the force-reflecting PHANToM interface.

1. INTRODUCTION

Two fundamental problems in remote manipulator teleoperation are free motions in Cartesian space and the contacting of the environment during task performance. Resolved-rate control (Whitney, 1969) is popular for free motion. However, rate control is not widely implemented in practice, perhaps due to the difficulty of rate control when the manipulator contacts the environment. If a constant rate is commanded while the manipulator contacts the environment, commanded joint angles integrate while actual joint angles are constrained until an unacceptably large wrench (force/moment vector) is exerted by the remote manipulator. The general problem of changing from free to constrained motion is termed the "phase transition problem" by Tarn et al. (1996) and is a current topic of research.

Raibert and Craig (1981) presented a hybrid control method wherein some Cartesian axes are controlled in position while the remaining axes are force controlled. While this method is effective in practical tasks, one must choose either position or force on each Cartesian axis. Whitney (1985) reviews various force control architectures. Hogan (1985) presented an impedance controller where the behavior of a manipulator is controlled to mimic a 6-degree-of-freedom (dof) Cartesian *m-c-k* system. The controller discussed in this paper, when in contact with the environment, is analogous to an impedance controller with only a damping term. In free motion, the controller acts like a rate controller. Most importantly, during the phase transition (the impact), the controller does not have to switch modes of control.

Colbaugh et al. (1993) present an adaptive scheme for controlling the end-effector impedance of robot manipulators in contact; however, an explicit control mode change is required for free motion. Hyde and Cutkosky (1994) experimentally evaluate several methods for controlling the transition from free motion to constrained motion, using a one-axis impact testbed. Yao and Tomizuka (1995) present an adaptive motion and force controller for manipulators with uncertainties in both the robot and contact surfaces. Vukobratovic et al. (1996) consider the problem of simultaneous stabilization of both the robot motion and interaction force in Cartesian space after contact in robotic tasks. Tarn et al. (1996) use an event-driven switching control strategy for robot impact control and force regulation where the instant of impact must be known. Tarn et al. state that control of manipulator impact and contact is an important current research area. They present an excellent literature review of the subject: all of the reviewed methods require an artificial control mode change in the transition from free motion to contact.

The current paper presents a method for dealing with the contact problem in teleoperation of remote manipulators, the Naturally-Transitioning Rate-to-Force Controller (*NTRFC*). The goal of this work is to provide a single controller which requires no artificial control modes changes in the transition from free motion to contact. Under commands from the operator via a master device, in free motion the manipulator moves with rate control, while in contact with the environment the wrench exerted on the environment is controlled. No artificial control mode or gain parameter changes are required so the transition is termed natural. A wrist-mounted force/torque (F/T) sensor and Force/Moment Accommodation (*FMA*) algorithm are required. Rate and *FMA* are active on all Cartesian axes simultaneously so no hybrid scheme is necessary. Since there are no artificial mode changes required, the threshold of contact is unimportant. A force-reflecting master may be used in conjunction with the *NTRFC* to increase the operator's sense of *telepresence* (the force-reflecting master is optional).

The *NTRFC* was originally developed experimentally at NASA Langley Research Center (Williams et al., 1996). It was implemented experimentally and proven very effective in completion of

representative space telerobotics tasks. We have expanded and implemented the *NTRFC* during the summers of 1997 and 1998 in an experimental system at Wright-Patterson AFB. The goal of this paper is to demonstrate the *NTRFC* concept via a modeling example and to present experimental results. Section 2 presents a description of the *NTRFC* algorithm, Section 3 presents a simple modeling example to demonstrate the concept, and Section 4 covers experimental implementation and results.

2. *NTRFC* DESCRIPTION

This section presents the Naturally-Transitioning Rate-to-Force Controller (*NTRFC*) concept. It is applicable to teleoperation of a remote manipulator with wrist-mounted force/torque (F/T) sensor, Cartesian rate inputs, and environment contact tasks.

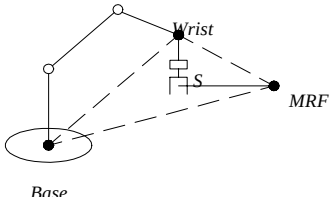

Figure 1. Manipulator Coordinate Frames

Figure 1 shows the manipulator coordinate frames used. The *Base* and *Wrist* frames are familiar. The Moving Reference Frame (*MRF*, denoted {*M*}) is the user-defined control frame. {*S*} is the F/T sensor frame. Figure 2 shows the *NTRFC* high-level control diagram. The two basic active ingredients are the resolved rate and force/moment accommodation (*FMA*) algorithms, described below. In addition, master devices enabling force-reflection can be used effectively, though this is not required in the *NTRFC*.

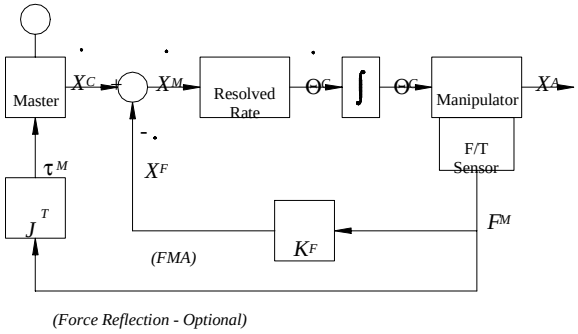

Figure 2. NTRFC Control Diagram

The resolved-rate algorithm is based on Whitney (1969). The manipulator Jacobian matrix *J* maps the joint rates to Cartesian rates $\dot{X}_M = J\dot{\Theta}_C$. In teleoperation, Cartesian rate inputs in {*M*}, $\dot{X}_M = \{v_M \quad \omega_M\}^T$ are commanded by the human using the master device. The rate equation is solved at each control step to calculate the instantaneous joint rates necessary to achieve the commanded Cartesian rate: $\dot{\Theta}_C = J^{-1}\dot{X}_M$. (Gaussian elimination is a more efficient and robust solution procedure than the matrix inverse). The *NTRFC* is also applicable to teleoperation of kinematically-redundant manipulators by replacing the matrix inverse with the matrix pseudoinverse. However, this case is not presented in the current paper. The joint rates are integrated to commanded joint angles Θ_C. The manipulator controller continuously servos to Θ_C; the actual Cartesian pose X_A results.

The resolved-rate algorithm is sensitive to singularities. When the determinant of *J* approaches zero, the matrix inverse is replaced by a matrix pseudoinverse based on Singular Value Decomposition (*SVD*) until the manipulator is through the singular neighborhood.

If the manipulator is in contact with its environment, there are constraints on X_A (the actual Cartesian pose in Fig. 2) and a Cartesian contact wrench exists. In this paper, *wrench* indicates a six-dof force/moment vector. A *force/moment accommodation* (*FMA*) algorithm has been implemented (simultaneously with the resolved-rate control) to automatically achieve zero wrench in order to minimize binding wrenches of contact during teleoperation. As discussed in the Introduction, this *FMA* algorithm is similar to an impedance controller (Hogan, 1985) with only the damping term. However, unlike the general impedance controller, the *FMA* algorithm is enabled during free and constrained motion.

A six-dof wrist-mounted F/T sensor reads the contact wrench $F_S = \{f_S \quad m_S\}^T$ at each control step. The weight and moment of the end-effector and payload must be subtracted from F_S, accounting for the configuration. In addition, the inertial wrench due to end-effector accelerations should also be subtracted to avoid spurious *FMA* in free motion. This inertial component is difficult to determine on-line due to the lack of acceleration feedback. However, in experimental implementation, we used a wrench deadband to avoid noise problems; this also masked the inertial loading at the low rates of acceleration performed experimentally. The feedback wrench must be in {*M*} so the modified sensor reading is transformed to the *MRF* wrench F_M via rigid body wrench transformations (Craig, 1989). This wrench is converted to a Cartesian rate $\dot{X}_F = K_F F_M$ and sent to the summing junction in Fig. 2. The diagonal gain matrix K_F has units *m*/*Ns* and *rad*/*Nms* for translational and rotational terms.

In the Naturally-Transitioning Rate-to-Force Controller (*NTRFC*), the resolved-rate algorithm is concurrently in operation with the *FMA* algorithm, for all Cartesian axes (no hybrid scheme is necessary). The overall resolved-rate input is the difference of the human-commanded rate and the *FMA* rate, $\dot{X}_M = \dot{X}_C - \dot{X}_F$. As the manipulator end-effector approaches a wall in the environment, the Cartesian rates commanded by the operator attempt to command motion through the wall, but the *FMA* controller commands a reverse motion to exert zero wrench. Therefore, an equilibrium condition is entered, where the displacement of the master device is proportional to the exerted Cartesian contact wrench. When the optional force-reflection is enabled by the master device, the wrench of the human hand on the master is proportional to the wrench exerted by the remote manipulator on the environment. The *NTRFC* automatically corrects misalignments so insertion tasks can be completed with minimum contact wrenches. If no *FMA* is used, it is difficult to complete tasks since the manipulator is "blind" in a wrench sense.

The teleoperated system behaves as a rate controller in free motion and as a simplified impedance controller in contact. The transition requires no mode changes, logical switches, or gain changes in the controller software or hardware and thus is termed a natural transition. The transition is a consequence of the physics of manipulator contact with the environment when using the control architecture of Fig. 2. Assuming a well-calibrated F/T sensor with sufficient wrench deadband, the *NTRFC* does not care when the moment of contact occurs. The *FMA* algorithm is enabled continuously (on all Cartesian axes, simultaneously with rate control on all Cartesian axes), but only

generates non-zero $\dot{X}_F$ in contact. The next section demonstrates the *NTRFC* concept.

3. *NTRFC* MODELING

This section presents dynamics and control modeling for a simple 1-dof 1*P* device in motion under the *NTRFC*. A basic *NTRFC* design procedure is outlined; this same procedure is expanded for real-world hardware in the next section. Since the free-motion to contact transition is a natural one, we must obtain desirable performance with only one set of gains and software control mode.

In hardware implementation the manipulator dynamics and environment characteristics are provided by the real world. For modeling, the *NTRFC* diagram in Fig. 2 must be modified to model these real world effects: 1) manipulator forward dynamics and forward kinematics must be calculated; 2) an environment model predicts the contact wrench F_M assuming a perfect F/T sensor and lumped environment characteristics; and 3) the operator-commanded manipulator Cartesian rate $\dot{X}_C$ is assumed to come from a fictitious teleoperation master device. The *FMA* algorithm is continuously enabled, but only generates non-zero $\dot{X}_F$ when the manipulator is in contact with the environment. The next subsection presents the general *NTRFC* design procedure, followed by modeling, *NTRFC* design, and simulation for the 1-dof 1*P* device.

3.1 *NTRFC* Design Procedure

The following *NTRFC* design procedure may be used for simulation and/or hardware implementation of a teleoperated manipulator system.

1) Design the remote manipulator controller to yield good, stable performance in free resolved-rate motion throughout the entire workspace. Any method may be used, including linearized independent PID joint control or feedback linearization with an optimal LQR controller.
2) Subject to the same manipulator free-motion controller structure and gains from above, determine *FMA* diagonal matrix gains K_F to ensure stable, desired transient and steady-state performance of the contact wrench given teleoperated Cartesian rate step inputs.
3) Determine system performance, sensitivity, and stability ranges. Simulate results. Implement in hardware. Iterate.

3.2 1*P NTRFC* Modeling

In this subsection we demonstrate the *NTRFC* concept and design procedure via a simple 1-dof device consisting of one prismatic joint (*P*). The 1*P* diagram is presented in Fig. 3. The device is modeled as a lumped mass m with viscous friction coefficient c_A. The relative device/environment compliance is modeled as a spring k_E and viscous damper c_E. The variable actuator length L_A operates along the X axis. The fixed length L_0 gives the distance along X from the origin to the undisplaced environment location. The Cartesian environment displacement variable x is measured from the end of L_0.

The 1*P* device has trivial resolved-rate ($J = J^{-1} = 1$) and forward kinematics (L_A is the total displacement along X) solutions. No rotations are possible. The dynamics equation of motion is:

$$f_A + f_M = m\ddot{L}_A + c_A\dot{L}_A \qquad (1)$$

where f_A and f_M are the actuator and Cartesian *MRF* contact forces. The Coriolis and centrifugal terms are zero for this 1-dof example.

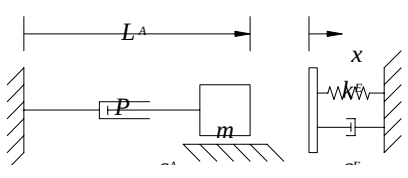

Figure 3. 1-dof 1P Device

The 1*P* *NTRFC* block diagram is given in Fig. 4 (in the Laplace domain). $\dot{x}_C$ is the modeled input from the human operator. Actual actuator length L_A is achieved by controller G_C servoing on length error $L_E = L_C - L_A$. In free motion, L_A is the output, $-L_0$ is ignored, and f_M is zero so the scalar *FMA* gain k_F has no effect. At the instant of contact we assume connection of the mass to the environment. In contact with the environment the input $\dot{x}_C$ exerts a force f_M on the environment after the transient dies out. Length L_0 is included after contact in simulation to provide the environment displacement variable $x = L_A - L_0$. In contact, both x and f_M are output variables of interest. The controller (a *PD* structure is chosen), 1*P* dynamics, and environment transfer functions are assumed to be linear:

$$G_C = k_P + k_D s \qquad G = \frac{1}{ms^2 + c_A s} \qquad G_E = -c_E s - k_E \qquad (2)$$

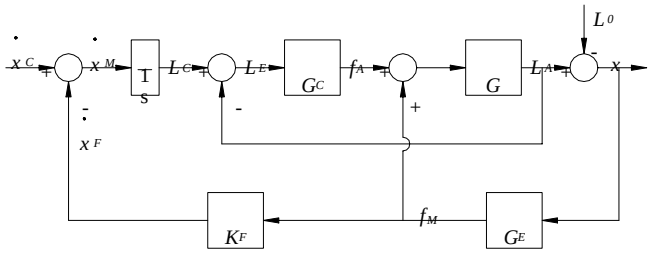

Figure 4. 1P NTRFC Block Diagram (no switches required)

The *NTRFC* design problem is stated: Given desired free-motion characteristics and desired contact force transient performance, calculate gains k_P, k_D, and then k_F. First, the *PD* controller is designed for good free motion of L_A given L_C from the resolved rate commands. The unconstrained (f_M=0) transfer function relating output L_A to input L_C is:

$$T(s) = \frac{L_A(s)}{L_C(s)} = \frac{k_D s + k_P}{ms^2 + (c_A + k_D)s + k_P} \qquad (3)$$

We specify 6% overshoot and 0.25 *sec* settling time for L_A in free motion; the desired characteristic polynomial is $s^2 + 80s + 3359.6$. It is difficult to calculate k_P and k_D via parameter matching due to the zero added by the *PD* controller. Therefore, we use an iterative approach to determine gains to satisfy the desired transient performance specifications; the result is k_P = 500 and k_D = 75. This concludes step one of the *NTRFC* design procedure.

Step two requires determination of *FMA* gain k_F for good contact force transient characteristics (the transition between rate and force control), given the same k_P and k_D gains. The in-contact transfer function relating output f_M to input $\dot{x}_C$ is now derived. The linear superposition principle is used to find the total contact force output f_M given the rate input $\dot{x}_C$ (with L_0=0) and the environment parameter $-L_0$ (with $\dot{x}_C = 0$):

$$T_{\dot{X}} = \frac{f_{M1}}{\dot{x}_C} = \frac{GG_CG_E}{s(1+GG_C-GG_E)+GG_CG_Ek_F}$$
$$T_L = \frac{f_{M2}}{L_0} = \frac{-s(1+GG_C)G_E}{s(1+GG_C-GG_E)+GG_CG_Ek_F} \quad (4)$$

$$f_M = f_{M1} + f_{M2} = T_{\dot{X}}\dot{x}_C - T_L L_0 \quad (5)$$

Substituting the transfer functions from Eq. 2 into Eq. 4, the closed-loop transfer function $T_{\dot{X}}$ for contact is (with L_0=0):

$$T_{\dot{X}} = \frac{-\left[k_Dc_Es^2 + (k_Dk_E + k_Pc_E)s + k_Pk_E\right]}{a_3s^3 + a_2s^2 + a_1s + a_0} \quad (6)$$

where:

$$a_3 = m$$
$$a_2 = c_A + c_E + k_D - k_Dc_Ek_F$$
$$a_1 = k_E + k_P - (k_Dk_E + k_Pc_E)k_F$$
$$a_0 = -k_Pk_Ek_F$$

The steady-state contact force and environment displacements are found using the final value theorem (separately for step inputs of magnitudes $\dot{x}_C$ and L_0):

$$f_{M1_{SS}} = \lim_{t\to\infty} f_{M1}(t) = \lim_{s\to 0} sf_{M1}(s) = \lim_{s\to 0} sT_{\dot{X}}\frac{\dot{x}_C}{s} = \frac{\dot{x}_C}{k_F} \quad (7)$$

Note this force is independent of the device and environment parameters. Similarly, $f_{M2_{SS}} = 0$. The steady-state force exerted on the environment by the 1*P* device after control has transitioned from rate to force and the corresponding steady state displacement (under the rate input command $\dot{x}_C$) are given below:

$$f_{M_{SS}} = f_{M1_{SS}} + f_{M2_{SS}} = \frac{\dot{x}_C}{k_F} \qquad x_{SS} = \frac{-f_{M_{SS}}}{k_E} = \frac{-\dot{x}_C}{k_Ek_F} \quad (8)$$

The stability of this system is determined via the Routh-Hurwitz criterion. Since the leading coefficient in the characteristic polynomial a_3=m is positive, all coefficients a_i must also be positive. Also, the ensuing entries in the first column of the Routh array must be positive. This leads to the following three conditions for stability:

$$\frac{k_D + c_E + c_A}{k_Dc_E} > k_F$$
$$ak_F^2 + bk_F + c > 0 \quad (9)$$
$$-k_Pk_Ek_F > 0$$

where:

$$a = k_Dc_E(k_Pc_E + k_Dk_E)$$
$$b = mk_Pk_E - (k_D + c_E + c_A)(k_Pc_E + k_Dk_E) - k_Dc_E(k_P + k_E)$$
$$c = (k_D + c_E + c_A)(k_P + k_E)$$

From the third condition in Eq. 9, the system is stable for $k_F < 0$ since k_P and k_E are always positive. The first condition is always met for $k_F < 0$ since the left-hand-side is always positive. For all cases simulated (including the example below), the quadratic condition did not dominate (i.e. k_F<d or k_F>e where both roots d and e are positive). However, this quadratic condition must be checked for all new cases.

Having determined the stability conditions and steady-state output variables, we have guidance for choosing k_F: k_F must be negative for stability and can be chosen for desired force amplification according Eq. 8 (left). However, the value of k_F has a significant effect on the transient force response. Therefore, it is preferable to adjust the force amplification through scaling rate commands $\dot{x}_C$ from the master device and to choose k_F for desired transient performance. This is demonstrated in the example below.

***1P* Simulation Example**

Given the following parameters, determine k_F and simulate 1*P NTRFC* motion. Above, the *PD* controller gains were determined for free motion: k_P=500 and k_D=75. The assumed device and environment parameters are (standard *SI* units are used): m=1; c_A=0.4; k_E=1,000; c_E=1; and L_0=0.10. A Matlab Simulink model was developed based on Fig. 4 to simulate 1*P NTRFC* motion. The $-L_0$ input is enabled only after contact. We varied k_F and studied the resulting transient performance. Three measures of transient performance were used: ±2% settling time, percent overshoot, and percent "wiggle". The first two are familiar, but must be obtained from the simulation data; second-order system formulas will not work since our system is third order, with two zeros. The third, percent wiggle, is a third order effect. It is defined to be the maximum one-cycle peak-to-peak amplitude, divided by the final value. This measure was instituted because some simulation results had zero percent overshoot, but significant "wiggle". For this example, Figs. 5 show these transient performance results. In each, the solid line represents the steady-state force results $f_{M_{SS}}$; the steady-state displacement transient results x_{SS} are very similar.

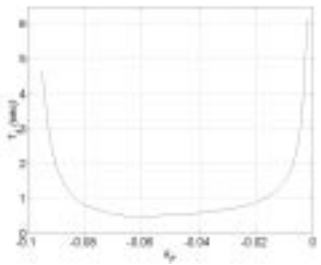

Figure 5a. Settling Time vs. k_F

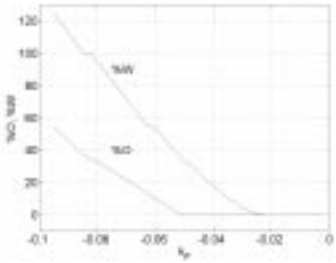

Figure 5b. %O and %W vs. k_F

To determine the best k_F for in-contact transient force performance, polynomial approximations were made for the simulation data in Figs. 5. Then we used an optimization procedure to determine the k_F which minimizes the objective function:

$$f(k_F) = k_1TS(k_F) + k_2PO(k_F) + k_3PW(k_F) \quad (10)$$

where k_i are the weighting factors giving the relative importance of settling time *TS*, percent overshoot *PO*, and percent wiggle *PW*. Percent wiggle is weighted more than overshoot; also given the difference in magnitude in settling time (relative to the two percent measures), settling time is weighted relatively heavier: k_1=75, k_2=1, and k_3=3. The optimal value of k_F was determined in this manner to be k_F = -0.0225. The associated settling time is 0.82 *sec*, and percent overshoot and wiggle are both 0%. Using this value in the simulation, Figs. 6 show the *NTRFC* simulation results for this example. In this simulation, the input $\dot{x}_C$ was linearly ramped from zero to a final value of 0.1 m/s (see Fig. 6a), to simulate a human operator commanding a constant rate starting from the master zero position. This figure also shows that the total resolved rate command $\dot{x}_M$ goes to zero in the steady-state, after the *FMA* rate $\dot{x}_F$ has been subtracted.

As shown in Fig. 6b, the actuator length L_A increases linearly under rate control in free motion, experiences transient behavior (difficult to see at this scale), and assumes a steady-state value after the natural transition from rate to force control. Figure 6c shows that the contact forces f_M are zero in free motion until contact; f_M also experiences transient behavior and assumes a constant steady-state force after the transition *even though the rate commands are still applied*. The steady state values calculated from Eq. 8 agree with the simulation results: $f_{M_{SS}} = 0.1/-0.0225 = -4.44$ and $x_{SS} = 0.00444$.

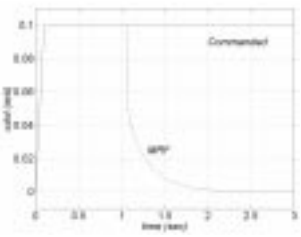

Figure 6a. NTRFC Rates

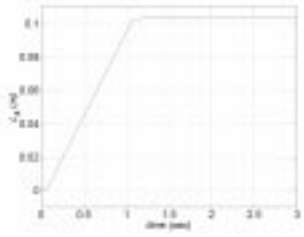

Figure 6b. Actuator Length L_A

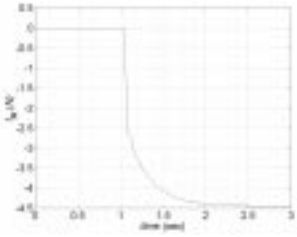

Figure 6c. Contact Force f_M

This example demonstrates the *NTRFC* concept and simulated response. One weakness is that the environment parameters have a strong effect on the transient performance, though the stability condition $k_F < 0$ is unchanged. We increased the environment parameters by an order of magnitude (k_E=10,000; and c_E=10) and obtained the new transient performance plots. These are similar in aspect to Figs. 5, but the k_F range is smaller, by a factor of 7.3 (note this is slightly less than the stiffness scaling of 10). With the stiffer environment, the percent overshoot and wiggle scales are unchanged. The settling time is slighter larger for the stiffer environment. Using the same weighting factors in Eq. 10, we determined the optimal gain to be k_F = -0.0041. The associated settling time is 2.30 *sec*, and percent overshoot and wiggle are 0% and 24.1%, respectively. The *NTRFC* behavior is similar to that of Figs. 6, but the settling time is higher, there is more percent wiggle (it is zero in Fig. 6c), and the steady state exerted force is larger due to the lower k_F.

In *NTRFC* design we have the following tradeoff. From Eq. 8 (left), a higher k_F leads to a lower exerted force. However, a lower k_F leads to better transient performance, within bounds. Therefore, we need to balance these competing factors; a scaling factor on the operator rate input $\dot{x}_C$ will help this.

In this simple example, the modeling is complex, and the transient performance is sensitive to k_F and the environment parameters. However, the exerted steady-state force is independent of the environment parameters. The *NTRFC* is implemented in a real-world system with a force-reflecting master in the next section.

4. PHANToM / Merlin Teleoperation with *NTRFC*

The *NTRFC* was implemented during summer 1998 in the Human Sensory Feedback (HSF) Laboratory of Wright-Patterson AFB. The master is a three-dof PHANToM haptic interface (Fig. 7) and the slave is a six-dof Merlin manipulator (Fig. 8). During summer 1997, the *NTRFC* was also implemented for the Merlin with a seven-dof force-reflecting exoskeleton master (Williams, 1997). The data below is from the PHANToM / Merlin system.

Figure 7. PHANToM

Figure 8. Merlin with Taskboard

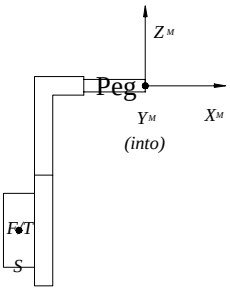

Figure 9. Merlin-Mounted Peg

Figure 10. Split Operator View

The PHANToM used has three encoders and three motors, so only translational rates were commanded and only force (no moment) feedback was provided to the operator. The task involved peg-in-the-hole insertions in a standard planar Fitts' law taskboard (Fitts and Peterson, 1964), with no need for orientation inputs. However, the full six-dof *FMA* algorithm was implemented, which provided automatic angular motion when moments were encountered due to misalignments. The Merlin-mounted peg is shown (with the F/T sensor which rigidly connects to the last manipulator link) in Fig. 9 and the Fitts' law taskboard is shown in Figs. 8 and 10. The L-shaped peg holder was designed for clear remote operator view. During the task, X_M is normal to the board, while Y_M-Z_M is in the plane of the board. In the data presented, the Merlin was teleoperated via rate commands $\dot{X}_C = \{v_C \quad 0\}^T$ (the operator-driven PHANToM position is taken to be v_C). Data runs were performed with various contact scenarios. The data below is from a single typical run, complete with noise and non-steady signals of the real world. Starting from an initial configuration, the Merlin peg (Fig. 9) was flown in free rate motion until contact was established in each of the *X*, *Y*, and *Z* directions. The operator attempted to maintain constant $\dot{X}_C$ during free and constrained phases of motion. The peg is mounted with a physical spring in the *X* axis, originally meant to protect against high forces in the insertion direction. Though this physical spring is no longer required with the software spring of the *FMA* algorithm, it was retained to demonstrate the *NTRFC* performs well with different environmental conditions (spring *X* and mostly rigid *Y* and *Z*).

Similar to the simulation example presented, it was found that the experimental system is stable for $k_{Fx}, k_{Fy}, k_{Fz} < 0$. However, unacceptable, though stable, transient contact transition can occur. The *NTRFC* gains are a 3*x*3 diagonal matrix K_F, tuned with equal diagonal components -0.0083. Figures 11 a, b, and c show the

operator-commanded rates $\dot{X}_C$, the Cartesian displacements *x*, *y*, and *z*, and the Cartesian contact forces. The results are in English units.

The operator attempts to hold constant rate inputs, starting at different times, $v_C = \{0.1 \quad -0.2 \quad -0.15\}^T$. The Cartesian displacements each display a constant velocity phase, followed by a transient transition, followed by a constant position phase. *y* is the sharpest, while *x* reaches its steady value gradually due to the hardware spring. The contact forces plot reveals all three directions contacted at nearly the same time (the peg was driven into a corner of the board, rather than a peg-hole). In free motion the forces are zero (or, noise and inertial loadings are within the deadband). At contact each rises to meet an approximately constant value. To the operator, the motion and contact looked and felt very smooth, with no notion of the variation seen in Fig. 11c. These results demonstrate the natural transition from rate to force control: in free motion, the displacement of the user's finger is proportional to the manipulator Cartesian rate; in contact, the force of the user's finger on the PHANToM (held at the same constant displacement) is proportional to the force exerted on the task board by the manipulator. No artificial controller switching is required. The steady-state force values can be calculated with the form of Eq. 8 (left): $f_{M_{SSX}} = 0.1/-0.0083 = -12$; $f_{M_{SSY}} = -0.2/-0.0083 = 24$; and $f_{M_{SSY}} = -0.15/-0.0083 = 18$. These values are achieved by experiment, as shown in Fig. 11c.

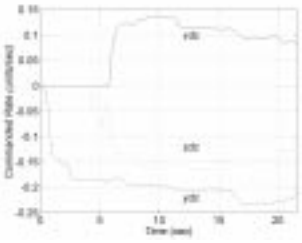

Figure 11a. Commanded Rates

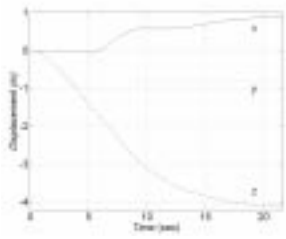

Figure 11b. Peg Displacements

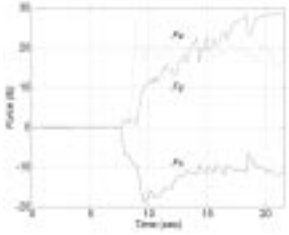

Figure 11c. Contact Forces

5. CONCLUSION

This paper has presented the Naturally-Transitioning Rate-to-Force Controller (*NTRFC*) for teleoperation of a remote manipulator. Existing rate control methods are often preferable to inverse position control in free motion, but unacceptable in contact with the environment due to integration of commands while under motion constraints, which builds up high contact wrenches. The *NTRFC* provides a method by which rate control in free motion naturally transitions to force control in contact. A force/moment accommodation (*FMA*) algorithm is the key ingredient. A wrist-mounted F/T sensor is required on the manipulator. The transition occurs due to the combination of the rate and *FMA* algorithms acting simultaneously on all Cartesian axes. No artificial control mode or gain changes are necessary, hence the method is insensitive to knowing the exact moment of contact in hardware implementation.

When a remote manipulator is teleoperated using the *NTRFC*, the following behavior results. In free motion, the displacement of the operator's hand with the master is proportional to the manipulator Cartesian rate. In contact, the displacement of the operator's hand is proportional to the Cartesian wrench exerted by the manipulator on the environment (control has transitioned naturally from rate to force). Furthermore, if the hand controller enables force-reflection to the operator, the wrench of the operator's hand reacting to the master force-reflection is proportional to the Cartesian wrench exerted by the manipulator on the environment.

A 1-dof 1*P* simulation example was presented to demonstrate the *NTRFC* concept. Then experimental results were presented from *NTRFC* implementation in the Human Sensory Feedback Laboratory of Wright-Patterson AFB. Future goals are: 1) Apply adaptive control techniques to lessen the dependence on models and environment parameter uncertainties; and 2) Develop analytical techniques for *NTRFC* design in nonlinear systems.

REFERENCES

R. Colbaugh, H. Seraji, and K. Glass, 1993, "*Direct Adaptive Impedance Control of Robot Manipulators*", Journal of Robotic Systems, 10(2): 217-248.

J.J. Craig, 1989, *Introduction to Robotics: Mechanics and Control*, Addison Wesley Publishing Co., Reading, MA.

P.M. Fitts and J.R. Peterson, 1964, "*Information Capacity of Discrete Motor Responses*", Journal of Experimental Psychology, 67(2): 103-112.

N. Hogan, 1985, "*Impedance Control: An Approach to Manipulation (3 parts)*", ASME Journal of Dynamic Systems, Measurement, and Control, 107:1-24.

J.M. Hyde and M.R. Cutkosky, 1994, "*Controlling Contact Transition*", IEEE Control Systems Magazine, 14(1): 25-30.

M. Raibert and J.J. Craig, 1981, "*Hybrid Position/Force Control of Manipulators*", ASME Journal of Dynamic Systems, Measurement, and Control, 103(2): 126-133.

T.J. Tarn, Y. Wu, N. Xi, and A. Isidori, 1996, "*Force Regulation and Contact Transition Control*", IEEE Control Systems Magazine, 16(1): 32-40.

M. Vukobratovic and R. Stojic, 1996, "*On Position/Force Control of Robot Interacting with Dynamic Environment in Cartesian Space*", ASME Journal of Dynamic Systems, Measurement and Control, 118(1): 187-92.

D.E. Whitney, 1969, *"Resolved Motion Rate Control of Manipulators and Human Prostheses"*, IEEE Transactions on Man-Machine Systems.

D.E. Whitney, 1985, *"Historical Perspective and State of the Art in Robot Force Control"*, IEEE International Conference on Automation and Robotics.

R.L. Williams II, 1997, "*Force-Reflecting Teleoperation Control Architecture*", Final Report, *AFOSR* Summer Faculty Program.

R.L. Williams II, F.W. Harrison, and D.I. Soloway, 1996, *"Naturally-Transitioning Rate-to-Force Controller for Manipulators"*, IEEE International Conference on Automation and Robotics, Minneapolis MN.

B. Yao and M. Tomizuka, 1995, "*Adaptive Control of Robot Manipulators in Constrained Motion - Controller Design*", ASME Journal of Dynamic Systems, Measurement and Control, 117(3): 320-328.